Horizon 2020
Programme

GENIORS

Research and Innovation Action (RIA)

This project has received funding from the European Union's Horizon 2020 research and innovation programme under grant agreement No 755171.

Start date : 2017-06-01 Duration : 48 Months
http://geniors.eu/

GENIORS

Report on dissolution model development

Authors : Mrs. Gilles LETURCQ (CEA)

GENIORS - Contract Number: 755171

Project officer: Roger Garbil

Document title	Report on dissolution model development
Author(s)	Mrs. Gilles LETURCQ
Number of pages	26
Document type	Deliverable
Work Package	WP7
Document number	D7.1
Issued by	CEA
Date of completion	2020-05-04 15:52:52
Dissemination level	Public

Summary

Several (U1-xPux)O2±? powders with different morphologies and different plutonium contents were synthetized using different synthesis routes. All the powders were fully characterized to quantify their structural parameters. After understanding verification of the morphological effects on mixed oxide dissolution , this study consists in quantifying the plutonium content effect on dissolution kinetics under same experimental conditions of dissolution (nitric acid 8.5M, 95°C). Significant differences in dissolution kinetics were observed. Indeed, the plutonium content is a key parameter that has to be considered in studies of (U1-xPux)O2±? dissolution kinetics. The effect of the plutonium content on dissolution kinetics was quantified and a kinetics law was established and validated to determine the experimental dissolution kinetics of an oxide whatever its morphology or its plutonium content, only for dissolutions in nitric acid 8.5M at 95°C.

Approval

Date	By
2020-05-04 15:53:42	Mrs. Gilles LETURCQ (CEA)
2020-05-04 16:22:46	Dr. Jean-Marc ADNET (CEA)
2020-05-19 08:03:00	Mr. Stéphane BOURG (CEA)

CONTENT

This project has received funding from the EURATOM research and training programme 2014-2018 under grant agreement No 755171. The content of this deliverable reflects only the author's view. The European Commission is not responsible for any use that may be made of the information it contains.

INTRODUCTION

The dissolution of spent nuclear fuel in nitric acid is one of the main steps of nuclear fuel recycling by hydrometallurgical process. For this purpose, it is useful to fully understand and quantify the impact of fuel characteristics on dissolution kinetics. In this study, a focus on the impact of the plutonium content of the oxide on dissolution kinetics was done. Only a few studies focused on this effect, because of the high radioactivity of these materials and the difficulties to manipulate plutonium.

Uriarte *et al.* [1] presented the differences in dissolution kinetics between UO_2 and PuO_2 in nitric medium. The authors described at 5 $mol.L^{-1}$ dissolution kinetic approximately twenty million times faster for UO_2 compared to PuO_2. For the mixed oxide, they explained that the more the mixed oxide contains plutonium the slower the dissolution kinetic. Lerch [2] described also a strong impact of the plutonium content on kinetics and solubility of the oxides. The author studied oxides with plutonium contents ranging from 15 to 25 percent. In this interval, the author proposed to model the impact of Pu amount on dissolution kinetics with a linear regression. Ikeuchi [3] studied the impact of plutonium content ranging from 18 to 29% on spent fuel. Irradiated MOX (Mixed OXides) with Pu content of 18% was estimated to be similar to irradiated fuel LWR (Light-Water Reactor) of FBR axial blanket fuel in term of solubility, although it contains less plutonium in composition Above a plutonium content of 18%, the author indicated an exponential decrease of the dissolution kinetics rate with a linear increase of plutonium content, and provided an empirical law also taking into account the acidity and temperature. Throughout the plutonium content range, Vollath [4] studied the oxide solubility at 6 hours by varying the dissolution acidity. The author observed no residue at the end of the dissolution of $(U_{1-x}Pu_x)O_{2\pm\Delta}$ mixed oxide with a plutonium content up to 40%. Over this value, the percentage of residues increases exponentially until reaching about 100% when the plutonium content is greater than 70%.

All these authors did not consider the effect of the morphology of the material on dissolution kinetics. In 1967, Molen tempted to describe the effect of specific surface area and crystallite size on PuO_2 dissolution kinetics without giving any empiric law. It was demonstrated both parameters had an impact [5]. Thus, no valid law has yet been determined describing the effect of the plutonium content on dissolution kinetics. Therefore, first, the effect of the morphology of the oxide on the dissolution rates has to be better understood. In a first part of this work, a study using different morphologies at the same plutonium content has been conducted to validate a morphological law on dissolution rates whatever the plutonium content. In a second part, tests on mixed oxides permit to define an empiric law describing perfectly the effect of the plutonium content on the dissolution rates taking care of the morphology of the samples.

SYNTHESES OF $(U,PU)O_2$ MODEL COMPOUNDS

In order to be able to model the dissolution of $(U,Pu)O_2$, single phase oxide powders were synthetized using different conversion routes, two oxalic routes, a sol/gel route and a calcination of PuO_2 colloids. Using different routes allowed obtaining oxides with the same Pu amount but exhibiting different morphologies, in order later to quantify the influence of this parameter on dissolution kinetics. Up to 18 different oxide powder batches were synthetized for a total of seven different compositions as shown in Figure 1. Typical morphologies obtained using the 4 different synthesis routes are shown in Figure 2. Depending on the oxalate precipitation parameters, needle morphology or platelet morphology can be targeted for the UO_2 and PuO_2. Then, the oxalic route permits only to obtain needle morphology mixed oxides for Pu amount less than 50% explaining why all Pu-richer samples were only obtained using sol/gel routes (SG).

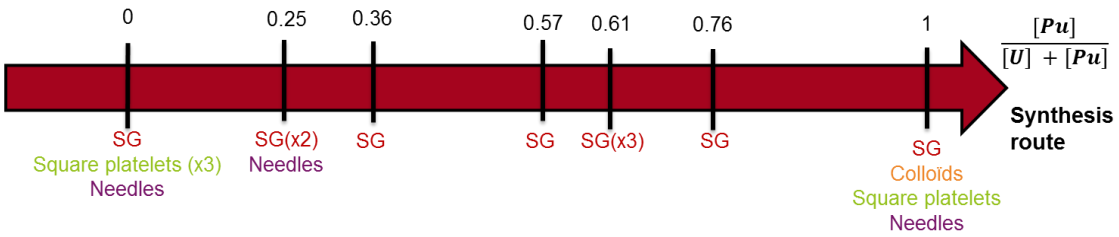

Figure 1 : Model compounds synthetized for dissolution studies.

This project has received funding from the EURATOM research and training programme 2014-2018 under grant agreement No 755171. The content of this deliverable reflects only the author's view. The European Commission is not responsible for any use that may be made of the information it contains.

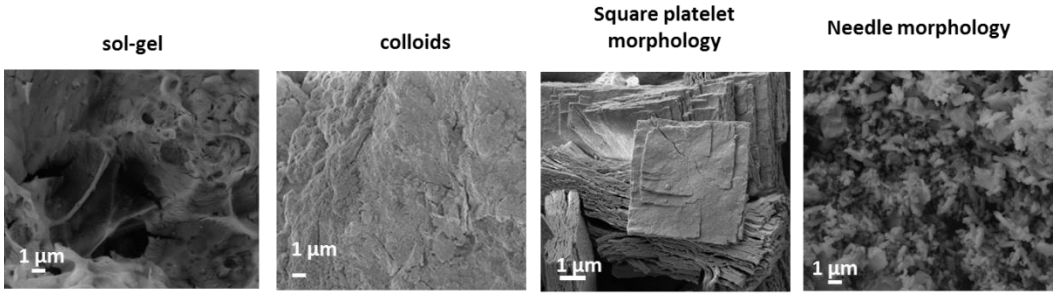

Figure 2 : morphologies of $(U,Pu)O_2$ powders obtained using the 4 different synthesis routes.

In order to modify the microstructure different calcination temperatures or atmospheres were applied to some compositions.

In a first paragraph the different synthesis routes are described, and then characterizations of the 18 samples are exposed in a second paragraph.

THE DIFFERENT SYNTHESIS ROUTES USED

The different synthesis routes used are known to produce single phase oxides and were chosen for this reason.

THE OXALIC SYNTHESIS ROUTE.

The oxalic precipitation apparatus is shown in Figure 3. Three reagents areneeded; the first one is composed of the cations to precipitate in a nitric solution. A total actinide concentration of about 30 $g.L^{-1}$ was used. The two other solutions are composed of a mixture of oxalic and nitric acids in defined proportions. The addition of the two first reagents inside a vortex created by stirring the third reagents leads to the precipitation of a single phase actinide oxalate. Thus, after filtering and rinsing the precipitate, calcination under a controlled atmosphere converts the precipitate onto the oxide.

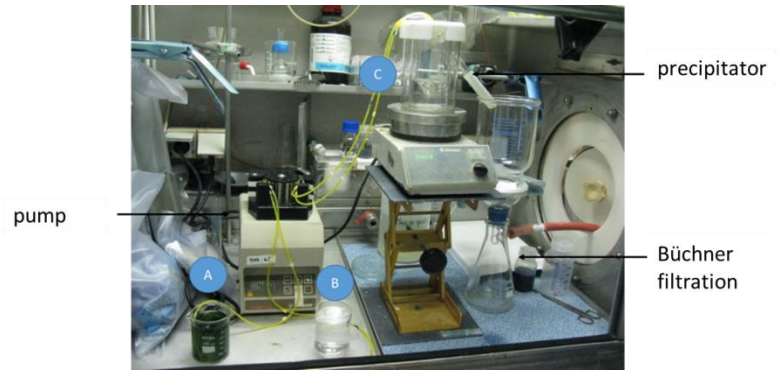

Figure 3 : Oxalic precipitation apparatus (example of uranium (IV) precipitation)

This project has received funding from the EURATOM research and training programme 2014-2018 under grant agreement No 755171. The content of this deliverable reflects only the author's view. The European Commission is not responsible for any use that may be made of the information it contains.

SQUARE PLATELET MORPHOLOGY

In industrial conditions, actinides (+IV) meanly precipitate as a $An^{IV}(C_2O_4)_2$, 6 H_2O P-1 triclinic oxalate with a shape of agglomerated square platelets. To form this oxalate $[HNO_3]$>2M and an oxalic excess have to be used. This synthesis route was used to fabricate UO_2 and PuO_2 samples.

NEEDLE MORPHOLOGY

Under different precipitation conditions, and addition of a monovalent cation NH_4^+ or $N_2H_5^+$, it is possible to precipitate $An^{IV}_2\ M_2^+(C_2O_4)_5{,}nH_2O$ (with An^{IV} = U ou Pu et M^+= H_3O^+, $N_2H_5^+$ or NH_4^+) exhibiting a hexagonal structure. Such compounds precipitate as agglomerated needles (Figure 4). The addition of M^+ on top of the use of different precipitation conditions allows the precipitation of these hexagonal oxalates for the synthesis of UO_2 and PuO_2 needle samples. For the synthesis of $(U,Pu)O_2$ by oxalic route, hydrazinium ions $N_2H_5^+$ were added to reduce and stabilize plutonium at its lower oxidation state (i.e. +III). In this case; the actinide solution, composed of a mixture of U^{IV}-Pu^{III}-$N_2H_5^+$, must have a plutonium ratio $\frac{[Pu]}{[U+Pu]}$ identical to the ratio targeted in the final oxide.

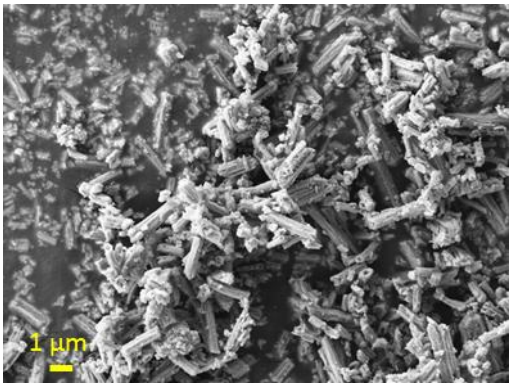

Figure 4: Micrography of $Pu^{IV}_2(NH_4)_2(C_2O_4)_5.nH_2O$ precipitate. (secondary electron mode)

THE SOL/GEL SYNTHESIS ROUTE

The sol/gel route that consists in the formation of a gel followed by calcination under a controlled atmosphere to form the oxide is commonly used [6] and [7]. This route allows the synthesis of mixed $(U,Pu)O_2$ for all Pu contents contrarily to the oxalic route. The protocol followed is slightly different to the one described in the literature [7] as the aim was to obtain powder and not beads. So, no silicon oil was used. The protocol is described in Figure 5. It requires very concentrated actinide solutions with as less as possible free nitric acid. Urea is used to complex Pu in order to delay its hydrolysis. HMTA decomposes at high temperature leading to NH_3 generation that causes actinide hydrolysis.

[Urea]/[U+Pu] and [HMTA]/[U+Pu] ratios of 1.7 and 2 respectively were used except for one sample (Pu/U+Pu = 55%). A [HMTA]/[U+Pu] ratio of 1.7 was used to make the gelation in a different pH. One sample was also calcined at 1000°C under Ar+100ppm O_2 to obtain an evolution of the microstructure.

This project has received funding from the EURATOM research and training programme 2014-2018 under grant agreement No 755171. The content of this deliverable reflects only the author's view. The European Commission is not responsible for any use that may be made of the information it contains.

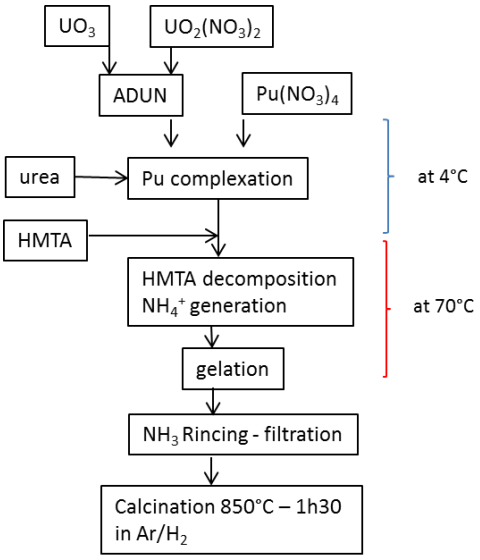

Figure 5: sol/gel process for $(U,Pu)O_2$ synthesis.

ACID DEFICIENT URANIUM NITRATE SOLUTION PREPARATION

In sol/gel route, uranium is added using ADUN solution. Such solution has a uranium concentration close to 700 $g.L^{-1}$ and a free acidity very low as its pH is around 1.8. To obtain such solution, some ammonium uranate is precipitated by addition of ammonia in uranium nitrate solution. UO_3 is then obtained by calcination under air atmosphere at 430°C of the precipitate. Then, this uranium trioxide is dissolved in a uranium nitrate solution.

THE PLUTONIUM RICH-SOLUTION

In order to concentrate a Pu nitrate solution without concentrating the free nitric acidity, a distillation column was used associated with many additions of as less acidic as possible nitric solution. Ideally, water should be used but the addition of water would cause Pu hydrolysis locally prior to the mixing of the solution. As shown in Figure 6, the more acidic the solution to be evaporated, the more acidic the vapor and the effective denitration [8]. Therefore, it is better to add little volumes of low acidic solution frequently than bigger volumes less often to keep the acidity of the solution to distillate as high as possible during the process of denitration.

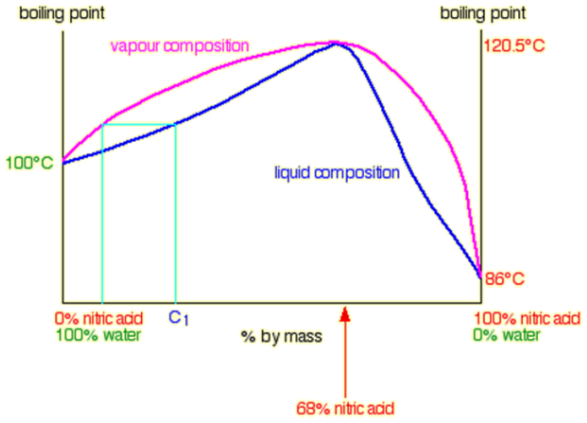

Figure 6: Distillation of nitric acid, link between acidity of the solution to be evaporated and the acidity of the vapor produced.

This project has received funding from the EURATOM research and training programme 2014-2018 under grant agreement No 755171. The content of this deliverable reflects only the author's view. The European Commission is not responsible for any use that may be made of the information it contains.

Addition of nitric solution of concentration below 0.5M causes Pu hydroxide colloids generation. Nitric acid of 0.5 M was then used. As described in Figure 6, the acidity of the solution to evaporate has to be higher than 3 M in order to evaporate more nitric acid than the 0.5 M added. Using this method, a Pu solution with [Pu] =510 $g.L^{-1}$ and [HNO_3] = 1.85 M was obtained. A picture of the nitric distillation apparatus is shown in Figure 7.

Figure 7: nitric distillation for concentration and denitration of a Pu solution

THE COLLOID SYNTHESIS ROUTE

As mentioned previously, addition of nitric acid less acid than 0.5 M in a Pu solution leads to colloid formation. [HNO_3] 0.1M was added to some Pu solution and then the colloidal suspension was filtered. Calcination at 850°C under air was then done to obtain another PuO_2 exhibiting a different morphology. Another calcination of a part of the batch was done at 1500°C under Ar+500ppmO_2 in order to modify the morphology.

CHARACTERISATIONS OF THE MODEL COMPOUNDS SYNTHETIZED

CHEMICAL COMPOSITION OF THE SAMPLES

Total dissolutions of a small quantity of each (U,Pu)O_2 sample were carried out using boiling HNO_3/HF (4 M/0.05 M). Then, $\frac{[Pu]}{[U+Pu]}$ ratio was determined for all the samples using TIMS (Thermal Ionization Mass Spectrometry) with a precision of 2 rel%. The results are given in Table 1. This determination was only done on sample calcined at 850°C. For samples calcined at different temperatures, it is assumed that no modification of the composition occurred during the second calcination.

Excepted for two samples, the analyzed chemical compositions were in agreement with respect to the targeted compositions. It has to be noted that using highly concentrated actinide solutions, little deviation in the volume used has a huge impact on the composition.

This project has received funding from the EURATOM research and training programme 2014-2018 under grant agreement No 755171. The content of this deliverable reflects only the author's view. The European Commission is not responsible for any use that may be made of the information it contains.

Table 1 : chemical composition of the $(U,Pu)O_2$ model compounds.

Synthesis route	N°	Targeted oxide	Obtained oxide
Needle oxalic route	1	$U_{0.75}Pu_{0.25}O_2$	$U_{0.75}Pu_{0.25}O_2$
Sol-gel route	2	$U_{0.75}Pu_{0.25}O_2$	$U_{0.75}Pu_{0.25}O_2$
	3	$U_{0.65}Pu_{0.35}O_2$	$U_{0.64}Pu_{0.36}O_2$
	4	$U_{0.45}Pu_{0.55}O_2$	$U_{0.43}Pu_{0.57}O_2$
	5	$U_{0.45}Pu_{0.55}O_2$	$U_{0.39}Pu_{0.61}O_2$
	6	$U_{0.35}Pu_{0.65}O_2$	$U_{0.39}Pu_{0.61}O_2$
	7	$U_{0.25}Pu_{0.75}O_2$	$U_{0.24}Pu_{0.76}O_2$

X-RAY DIFFRACTION

All the oxides synthetized were analyzed by XRD. All the samples are single phase oxides with a fluorine cubic structure and are well crystallized. As examples, XR diffraction patterns of oxides obtained via sol-gel route are shown in Figure 8. No impurities were observed.

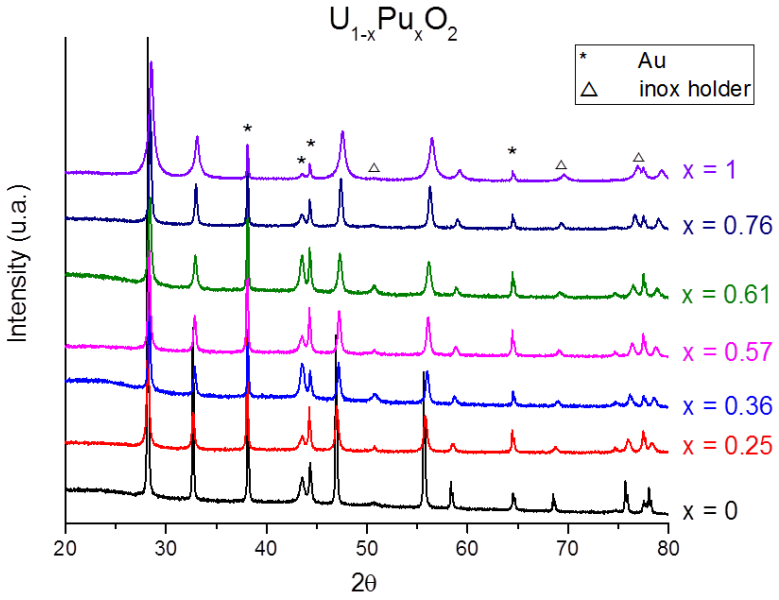

Figure 8: X-Ray Diffraction patterns on oxides made using sol-gel route

The lattice parameters were determined by Le Bail refinement using the TOPAS software (TOtal Pattern Analysis Solutions) from BRUKER AXS [9] where only the profile parameters (cell dimensions, peak shapes, background, zero point correction) were refined. The microstrains and average crystallite sizes were calculated with the fundamental parameters method [10]. Results are given in Table 2.

This project has received funding from the EURATOM research and training programme 2014-2018 under grant agreement No 755171. The content of this deliverable reflects only the author's view. The European Commission is not responsible for any use that may be made of the information it contains.

Table 2: XRD refinements on model compounds.

Compound	Synthesis route	Sample Name	Cell parameter (Å)	Crystallite size (nm)	microstrains (%)	O/M
UO_2	Needle oxalic route	UO_2 P Ar	5.4688 (1)	161 (4)	0.1 (0)	2.02 ± 0.02
	Square platelet oxalic route	UO_2 P Ar/H_2	5.4704 (1)	167 (3)	0.1 (0)	2.01 ± 0.02
	Square platelet oxalic route	UO_2 P air+Ar/H_2	5.4686 (2)	360 (8)	0.1 (0)	2.03 ± 0.02
	Needle oxalic route	UO_2 B	5.4704 (2)	129 (8)	0 (0)	2.01 ± 0.02
	Sol-gel	UO_2 SG	5.4694 (1)	164 (2)	0.1 (0)	2.02 ± 0.02
$U_{0,75}Pu_{0,25}O_2$	Needle oxalic route	25% B	5.4497 (2)	66 (1)	0.2 (0)	2.01 ± 0.02
	Sol-gel	25% SG YZ	5.4512 (1)	46 (1)	0.3 (1)	2.01 ± 0.02
	Sol-gel	25% SG GL	5.4493 (2)	34 (1)	0.1 (0)	1.99 ± 0.02
$U_{0,64}Pu_{0,36}O_2$	Sol-gel	36% SG	5.4412 (2)	48 (1)	0.2 (0)	2.00 ± 0.02
$U_{0,45}Pu_{0,57}O_2$	Sol-gel	57% SG	5.4276 (1)	49 (1)	0.3 (1)	2.02 ± 0.02
$U_{0,39}Pu_{0,61}O_2$	Sol-gel	61% SG a	5.4321 (1)	43 (1)	0.2 (0)	1.92 ± 0.02
$U_{0,39}Pu_{0,61}O_2$	Sol-gel	61% SG b	5.4228 (1)	33 (1)	0.3 (0)	2.01 ± 0.02
$U_{0,39}Pu_{0,61}O_2$	Sol-gel 1000°C	61% SG c	5.4241 (1)	69 (2)	0.1 (0)	2.00 ± 0.02

This project has received funding from the EURATOM research and training programme 2014-2018 under grant agreement No 755171. The content of this deliverable reflects only the author's view. The European Commission is not responsible for any use that may be made of the information it contains.

$U_{0,24}Pu_{0,76}O_2$	Sol-gel	76% SG	5.4131 (1)	56 (2)	0.3 (1)	2.04 ± 0.02
PuO_2	Sol-gel	PuO_2 SG	5.3980 (1)	17 (1)	0.1 (0)	1.98 ± 0.02
	Needle oxalic route	PuO_2 B	5.3958 (2)	75 (2)	0.2 (0)	2.00 ± 0.02
	Square platelet oxalic route	PuO_2 P	5.3960 (1)	92 (3)	0.2 (0)	2.00 ± 0.02
	Colloïd route	PuO_2 C	5.3969 (1)	270 (15)	0	1.99 ± 0.02

The lattice parameters vary with the plutonium content according to the Vegard's law (Equation 1). This law was plotted in Figure 9 from the values presented by Young *et al.*[11] for UO_2 and Freeman *et al.*[12] for PuO_2. The experimental lattice parameters are nearly perfectly aligned with this law, indicating that they correspond to the theoretical lattice parameters calculated from the TIMS characterization. In the case of $U_{0.39}Pu_{0.61}O_{2\pm\delta}$ SG a, there is a slight deviation from the line corresponding to a slight sub-stoichiometry of the compound, as already seen in Table 2

$$a_{theoretical} = -0.071 * \frac{[Pu]}{[U+Pu]} + 5.467 \qquad \text{Equation 1}$$

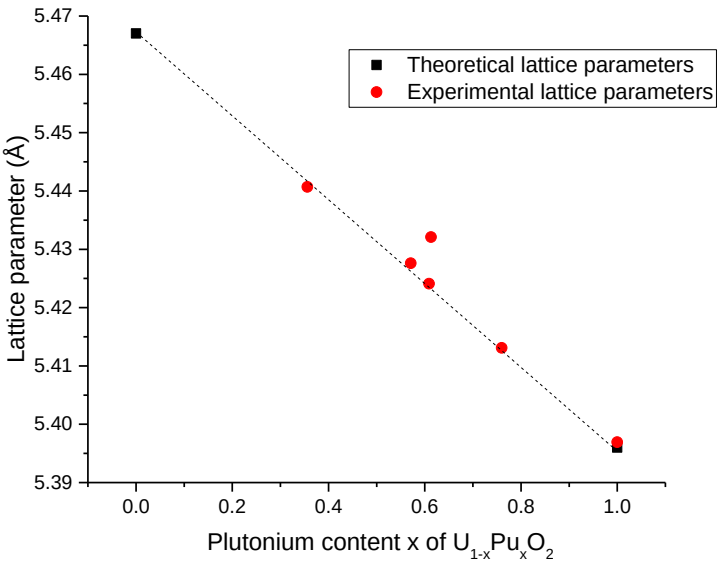

Figure 9 : Evolution of the lattice parameter with Pu content in $(U,Pu)O_2$ solid solution, measured by XRD and compared with Vegard's law.

This project has received funding from the EURATOM research and training programme 2014-2018 under grant agreement No 755171. The content of this deliverable reflects only the author's view. The European Commission is not responsible for any use that may be made of the information it contains.

This deviation from Vegard's law can be traduced by, the difference between the experimental and the calculated/theoretical lattice parameter and can be explained by an oxygen stoichiometric variation. From the experimental lattice parameter, it is possible to calculate the oxygen stoichiometry of the oxide $(U_{1-x}Pu_x)O_{2\pm\delta}$ from the empiric law (**Equation 2**) [13].The fourth column of the table 1 shows the results of this calculation for each material, leading to a perfect stoichiometry, with the uncertainty, for each compound.

$$\delta = \frac{5.467 * (1 - x) + 5.396x - a_{experimental}}{0.112} \qquad \textbf{Equation 2}$$

Excepted one sample (61% sol-gel) the O/M ratios were found to be close to 2.00. For this specific sample the oxide appears to be under stoichiometric indicating a partial reduction of Pu.

Microstrains are very low and all in the same order of magnitude.

The oxides resulting from the same calcination temperature presents similar average crystallite sizes (Table 2). Furthermore, the average crystallite sizes seem to increase with the precursors calcination temperature, in accordance with data from the literature describing crystal growth during the sintering process [14].

SPECIFIC SURFACE AREAS DETERMINED BY BET METHOD

The specific surface areas of all the oxides were determined using BET method with nitrogen (Table 3), all the values range from 0.2 to 6 3 $m^2.g^{-1}$. The specific surface areas obtained are rather small, but in accordance with the values already obtained in the literature for actinide oxides [15]. Specific surface area of the oxides appears to be lower when the calcination temperature applied to obtain the oxide is high.

Table 3: Specific surface area determined by BET method using nitrogen.

Compound	Synthesis route	Sample name	SSA ($m^2.g^{-1}$)
UO_2	Square platelet oxalic route	UO_2 P Ar	1 ± 0.2
	Square platelet oxalic route	UO_2 P Ar/H_2	1 ± 0.3
	Square platelet oxalic route	UO_2 P air+Ar/H_2	1 ± 0.3

This project has received funding from the EURATOM research and training programme 2014-2018 under grant agreement No 755171. The content of this deliverable reflects only the author's view. The European Commission is not responsible for any use that may be made of the information it contains.

	Needle oxalic route	UO_2 B	2 ± 0.2
	Sol-gel	UO_2 SG	2 ± 0.2
$U_{0,75}Pu_{0,25}O_2$	Needle oxalic route	25% B	2.8 ± 0.2
	Sol-gel	25% SG YZ	1 ± 0.2
	Sol-gel	25% SG GL	0.2 ± 0.2
$U_{0,64}Pu_{0,36}O_2$	Sol-gel	36% SG	0.4 ± 0.2
$U_{0,45}Pu_{0,57}O_2$	Sol-gel	57% SG	0.4 ± 0.3
$U_{0,39}Pu_{0,61}O_2$	Sol-gel	61% SG a	1 ± 0.1
	Sol-gel	61% SG b	1.5 ± 0.3
	Sol-gel 1000°C	61% SG c	0.9 ± 0.2
$U_{0,24}Pu_{0,76}O_2$	Sol-gel	76% SG	2.2 ± 0.2
PuO_2	Sol-gel	PuO_2 SG	6.3 ± 0.5
	Needle oxalic route	PuO_2 B	2.7 ± 0.4
	Square platelet oxalic route	PuO_2 P	3.3 ± 0.4
	Colloïds	PuO_2 C	0.2 ± 0.2

SEM IMAGES

The different UO_2 microstructures obtained are presented in Figure 10. Relative observations on these samples are summarized inTable 4. For all these oxides the crystallite sizes observed using SEM are in agreement with the crystallite sizes determined by XRD refinements. The UO_2 synthetized using sol-gel route is composed of big porous aggregates. For the three compounds obtained by conversion of $U^{IV}(C_2O_4)_{2,6}H_2O$ the square platelet sizes vary from 4 to 8 µm except for the sample calcined twice for which the grain size is increased by a factor two due to the increase of the total calcination duration. For this powder an intergranular porosity is also observed, probably due to the U_3O_8 reduction onto UO_2. U_3O_8 cristallises in a 30% bigger cell than UO_2[16]. Thus, the second thermal treatment may have not been long enough or been done at a too low temperature to totally

This project has received funding from the EURATOM research and training programme 2014-2018 under grant agreement No 755171. The content of this deliverable reflects only the author's view. The European Commission is not responsible for any use that may be made of the information it contains.

remove this intergranular porosity. The last UO_2 sample is composed of big agglomerates of little hexagonal needles as expected for the conversion of $U_2M_2(C_2O_4)_5,nH_2O$ (avec $M^+ = H_3O^+$, $N_2H_5^+$).

Table 4: SEM observations on UO_2 samples

	Synthesis route and calcination	Name	Aggregate size (µm)	Grain size (nm)	Comments
1	Sol-gel Ar/H_2 (96/4)	UO_2 SG	216 ± 56	~ 200	Big porous aggregates
2	Square platelets oxalic route Air + Ar/H_2 (96/4)	UO_2 P Air+Ar/H_2	6 ± 2	300-800	Intergranular porosity
3	Square platelets oxalic route Ar	UO_2 P Ar	6 ± 2	150-400	Ø
4	Square platelets oxalic route Ar/H_2 (96/4)	UO_2 P Ar/H_2	6 ± 2	150-400	Ø
5	Needles oxalic route Ar	UO_2 B	18 ± 15	~ 100	Agglomerated needles

This project has received funding from the EURATOM research and training programme 2014-2018 under grant agreement No 755171. The content of this deliverable reflects only the author's view. The European Commission is not responsible for any use that may be made of the information it contains.

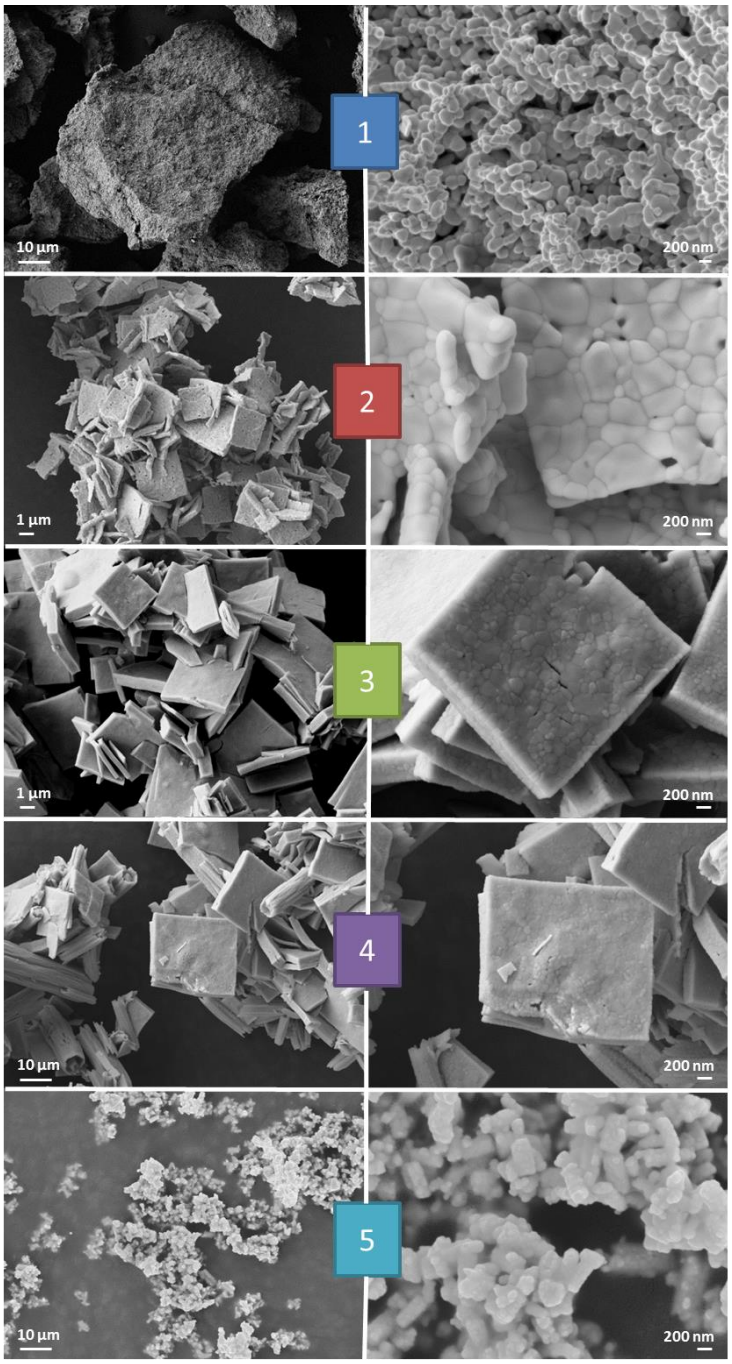

Figure 10: secondary electron micrographies of UO_2 synthetized using the different conversion routes. Numbers being those reported in Table 4.

Table 5 and Figure 11 are relative to the other samples made using oxalic routes. The square platelets of PuO_2 have similar sizes to those observed on UO_2. However, the grain size looks smaller. The two other samples are composed of hexagonal needles of several tens of µm. Their grain sizes are in agreement with the crystallite sizes determined by XRD refinements (tens of nm).

This project has received funding from the EURATOM research and training programme 2014-2018 under grant agreement No 755171. The content of this deliverable reflects only the author's view. The European Commission is not responsible for any use that may be made of the information it contains.

Table 5: SEM observations linked to Figure 11.

	Synthesis route and calcination	Name	Aggregate size (µm)	Grain size (nm)	Comments
1	PuO_2 Square platelet oxalic route Ar	PuO_2 P	7 ± 1	50 - 100	Square platelets
2	PuO_2 Needles oxalic route Ar	PuO_2 B	25 ± 5	< 100	Hexagonal needle agglomerates
3	$U_{0,75}Pu_{0,25}O_2$ Needles oxalic route Ar	25% B	108 ± 55	n.d.	Hexagonal needle agglomerates

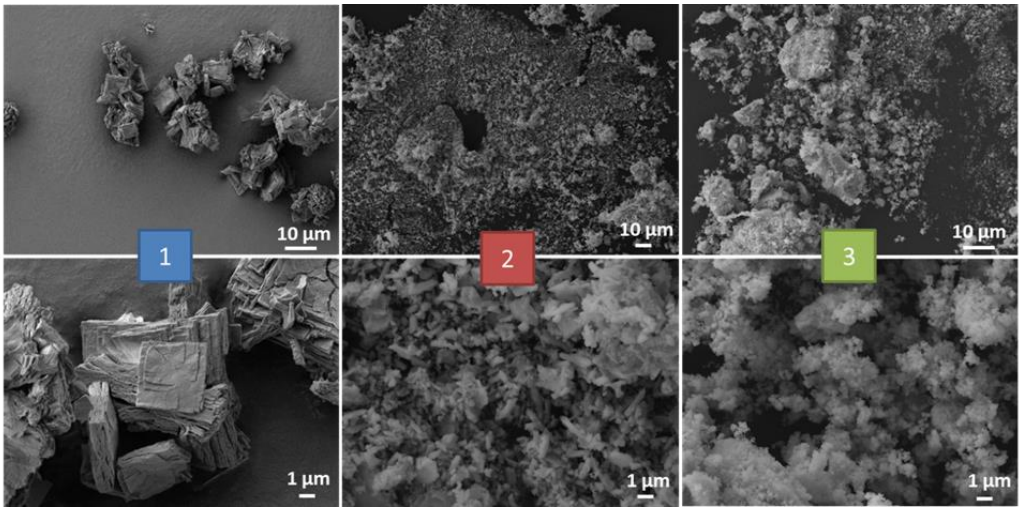

Figure 11: secondary electron micrographies of other samples synthetized using the oxalic routes. Numbers being those reported in Table 5.

Oxide compounds of Figure 12 and Table 6 are mixed oxides or PuO_2 made using sol-gel route. For all these samples, crystallite sizes are too small to be observed by SEM (<100nm). This is in agreement with the values determined by XRD refinements. All these samples are composed of big porous agglomerates (several hundreds of µm long).

This project has received funding from the EURATOM research and training programme 2014-2018 under grant agreement No 755171. The content of this deliverable reflects only the author's view. The European Commission is not responsible for any use that may be made of the information it contains.

Table 6: SEM observations linked to Figure 12

	Synthesis route and calcination	Name	Aggregate size (µm)	Grain size (nm)	Pore size (µm)	Comments
1	$U_{0,75}Pu_{0,25}O_2$ Sol-gel Ar/H_2 (96/4)	25% SG YZ	207 ± 33	Ø	2	Big porous aggregates
2	$U_{0,43}Pu_{0,57}O_2$ Sol-gel Ar/H_2 (96/4)	57% SG	97 ± 55	Ø	0.90	Big porous aggregates
3	$U_{0,24}Pu_{0,76}O_2$ Sol-gel Ar/H_2 (96/4)	76% SG	75 ± 75	Ø	0.75	Big porous aggregates
4	PuO_2 Sol-gel Ar/H_2 (96/4)	PuO_2 SG	63 ± 41	Ø	Ø	Big porous aggregates

This project has received funding from the EURATOM research and training programme 2014-2018 under grant agreement No 755171. The content of this deliverable reflects only the author's view. The European Commission is not responsible for any use that may be made of the information it contains.

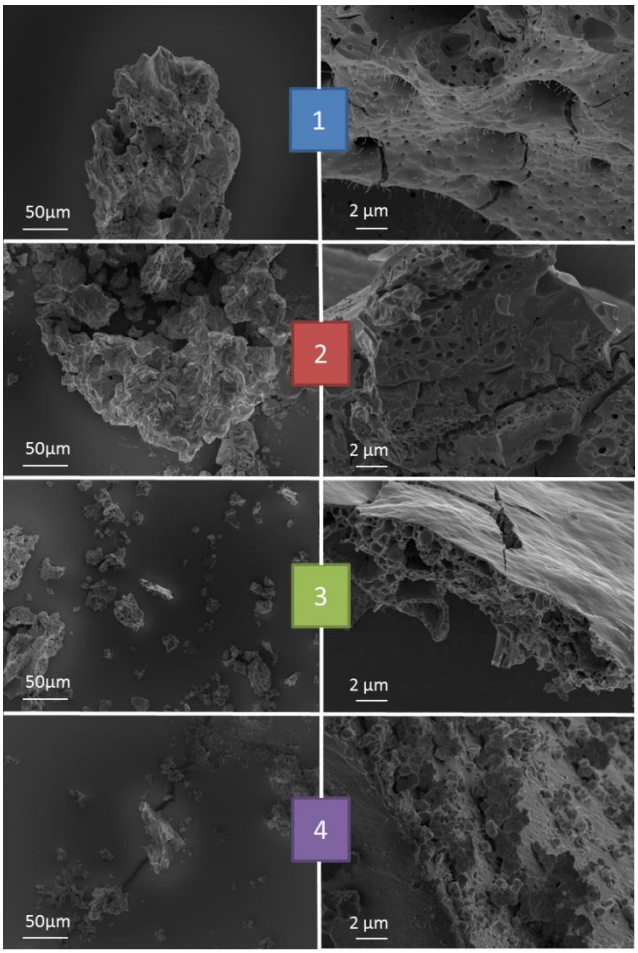

Figure 12: secondary electron micrographies of samples synthetized using the sol-gel routes. Numbers being those reported in Table 6.

EDX analyses were also done to verify the homogeneity of all the samples. All the results are in agreement with the composition analyzed by TIMS on total dissolution liquors within an uncertainty of 5% due to a lack of flatness of unpolished powder samples. It is then possible to conclude on the homogeneity of all the samples.

SEM images in secondary electron mode of PuO_2 obtained by calcination at 1500°C of colloids are shown in Figure 13. The sample is composed of sintered grain agglomerates with a size over 1mm long. Some intra and intergranular pores of several hundreds of nm long are also observed.

This project has received funding from the EURATOM research and training programme 2014-2018 under grant agreement No 755171. The content of this deliverable reflects only the author's view. The European Commission is not responsible for any use that may be made of the information it contains.

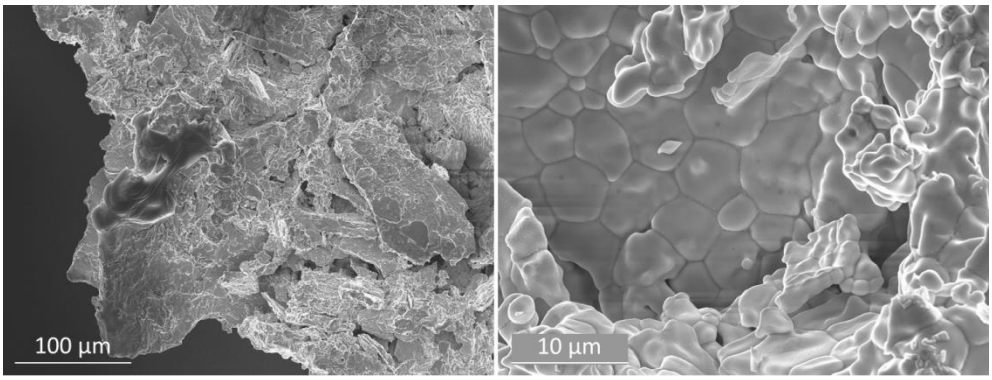

Figure 13: secondary electron micrographies of PuO_2 made by calcination at 1500°C of colloids.

In conclusion, eighteen different actinide samples were synthetized and fully characterized in order to be able to study dissolution in function of morphology and Pu amount.

EFFECT OF MORPHOLOGY PARAMETERS ON DISSOLUTION KINETICS

Dissolution experiments were carried out after setting up the dissolution apparatus in a glove box (**Figure 14**). First, effects of morphology characteristics of powder were tested using the oxides for which several samples were obtained ie PuO, $U_{0.39}Pu_{0.61}O_2$, UO_2 and $U_{0.75}Pu_{0.25}O_2$. Each dissolution test was conducted in a dissolution reactor of 60 mL with 15 mL of nitric acid and 300 mg of oxide powder. The lid of the reactor was equipped with a cooling column allowing potential nitrous vapors to condense. For safety issues the top of this cooling column was connected to a gas cleaner composed of soda 2 M to ensure no nitrous emission inside the globe box. The solution was heated using a hot plate; temperature was followed using a thermometer. The solution was homogenized using a magnetic stirrer at 300 rpm. Once the solution at the right temperature, the oxide powder was introduced inside the reactor at t=0. Then, aliquots of the dissolution liquor were sampled using a syringe and analyzed by alpha counting to follow the dissolution kinetics.

This project has received funding from the EURATOM research and training programme 2014-2018 under grant agreement No 755171. The content of this deliverable reflects only the author's view. The European Commission is not responsible for any use that may be made of the information it contains.

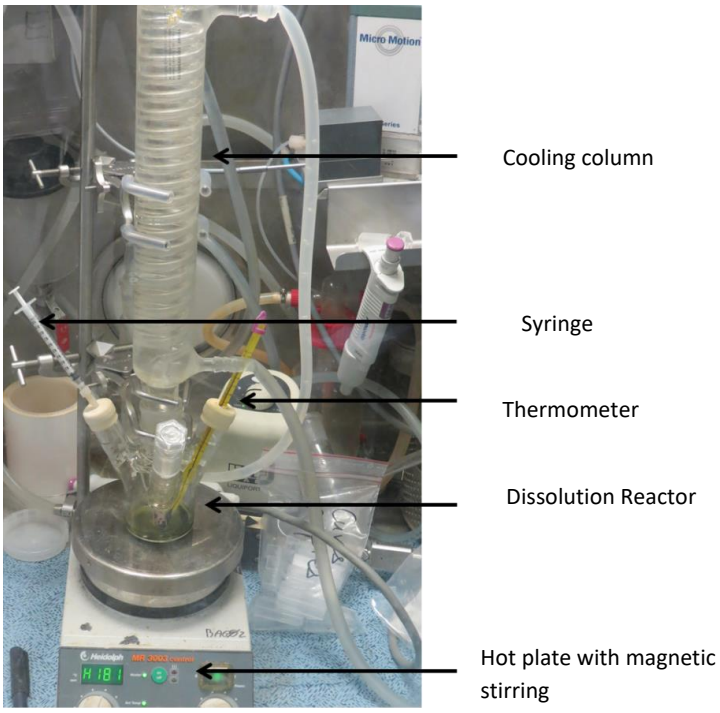

Figure 14: Dissolution apparatus set up in glove box

DISSOLUTION OF PuO_2 IN NITRIC ACID 8.5M AT 95°C

In order to determine the impact of the morphology of the PuO_2 powder on its dissolution kinetics, dissolution tests were carried out using [HNO_3] 8.5M at 95°C on the four different PuO_2 samples previously synthetized. Characterization parameters of these 4 PuO_2 powder samples are given in **Table 7**. Dissolution tests were conducted for 6 h. At the end, dissolution liquors remained colorless (**Figure 15**) reflecting the very low dissolution kinetics of PuO_2 even in very aggressive conditions, as it is already well known. At the end of the dissolution experiments more than 90 % of the powders were recovered after filtration.

Table 7: Morphological characteristics of PuO_2 powders.

Compound	Precursors route	Average crystallite size (nm)	Specific surface area ($m^2.g^{-1}$)
1	Sol-gel 850°C	17 (1)	6.3 ± 0.5
2	Sol-gel 1500°C	270 (15)	0.2 ± 0.2
3	Oxalic platelets	92 (3)	3.3 ± 0.4
4	Oxalic sticks	75 (2)	2.7 ± 0.4

This project has received funding from the EURATOM research and training programme 2014-2018 under grant agreement No 755171. The content of this deliverable reflects only the author's view. The European Commission is not responsible for any use that may be made of the information it contains.

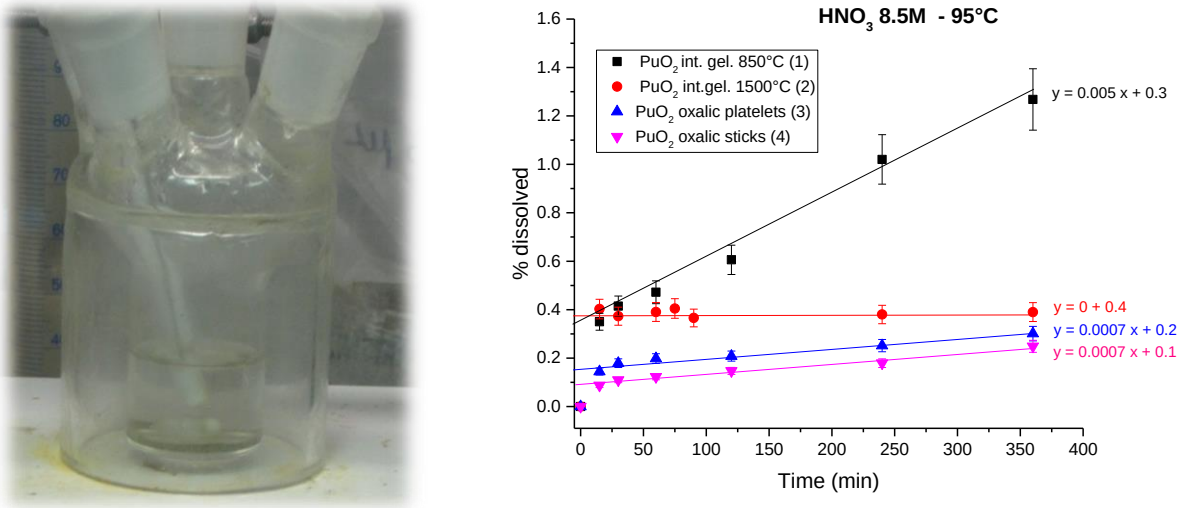

Figure 15 : Picture of dissolution of PuO_2 sample in HNO_3 8.5M 95°C after 6h (left) Dissolution kinetics of PuO_2 powders in HNO_3 8.5M – 95°C. (right)

Dissolution kinetics rates are plotted in **Figure 15**. The determination of the plutonium concentration in solution allows determining the mass of dissolved plutonium dioxide and thus the percentage of powder dissolved at each time. All these percentages lead to a straight line and by linear regression, the slope of the line corresponds to the dissolution kinetics rate. An initial dissolution kinetics regime is observed corresponding probably to an erasing of the crystalline defects more reactive with respect to dissolution and is expressed by the non-nil y-intercepts.

Sample 1 obtained by internal gelation calcined at 850°C has the higher dissolution kinetics in agreement with the morphology parameters (higher specific surface area and smaller crystallite size). Then, both samples obtained by oxalic route have similar dissolution kinetics whatever the platelet or stick morphology despite different specific surface area and crystallite size values. It seems that the effects of these two parameters annihilate each other to lead to similar dissolution behavior for both samples. Finally, PuO_2 obtained by internal gelation calcined at 1500°C exhibit dissolution kinetics rate close to nil. This powder has very low specific surface area and a crystallite size sixteen times higher than the same sample calcined at 850°C that can explain this dissolution resistance.

Based on these data it was possible to establish a kinetics law with respect to the two morphology parameters (specific surface area and crystallite size) for these 4 samples:

$$r\ PuO_2 = k * SSA^{0,33} * Sc^{-1}$$ **Equation 3**

with r : dissolution kinetic (%dissolved / min) ; k=0.04 , SSA: specific surface area ($m^2.g^{-1}$) ; S_C: average crystallite size (nm)

The correlation coefficient associated with this formula is 0.96. This coefficient is acceptable considering the errors of the quantification of the powder average crystallite sizes and specific surface areas.

DISSOLUTION OF $U_{0.39}PU_{0.61}O_2$ IN NITRIC ACID 8.5M AT 95°C

Similar dissolution tests were carried out on the three uranium plutonium mixed oxides with 61% of Pu but exhibiting different morphologic parameters (SSA and S_C). The same protocol was used. The congruence of

This project has received funding from the EURATOM research and training programme 2014-2018 under grant agreement No 755171. The content of this deliverable reflects only the author's view. The European Commission is not responsible for any use that may be made of the information it contains.

uranium and plutonium was verified and the mixed powders dissolve homogeneously. The kinetics rates of dissolution are shown in Figure 16. The figure shows that for a same plutonium content, the dissolution rate can vary by a factor of 4 only due to morphological differences.

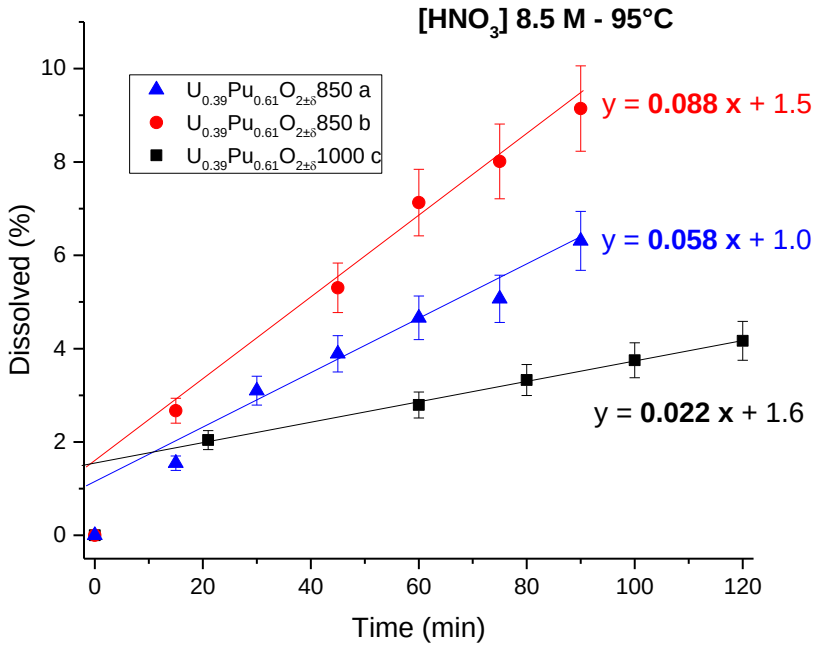

Figure 16 : Dissolution of three$U_{0.39}Pu_{0.61}O_2$ powders, in 8.5 mol.L^{-1} nitric acid at 95°C.

Keeping the same partial orders for the crystallite size and the specific surface area than determined in PuO_2 model (ie -1 and 0.33 respectively), the resolution of the system of three equations with an unknown leads to the empirical law Equation 4. The correlation coefficient of this law is 0.99. This coefficient expresses the possibility to describe satisfactorily the kinetics of dissolution from the morphological characteristics of the powders.

$$r = 10^{0,35} * Sc^{-1} * SSA^{0,33}$$ Equation 4

With Sc the crystallite size in nm and SSA the specific surface area in $m^2.g^{-1}$.

DISSOLUTION OF UO_2 SAMPLES

Similar approach has to be used for the different UO_2 samples. However, UO_2 is known to dissolve more easily. So less aggressive conditions had to be used in order to be able to follow its dissolution kinetics. Acidity was reduced first to 5 then 3 mol.L^{-1} but still dissolution was too fast. Finally, dissolution were carried out using nitric 1.5 mol.L^{-1} at 50°C. Uranium concentrations were determined using uv vis spectroscopy.

Once again, dissolution kinetics appeared to be linear until full dissolution as shown in Figure 17. Three different kinetics were observed for the 5 tests despite all led to full dissolution within an hour. A first kinetics of about 5 to 6% dissolved per minute corresponds to samples obtained via sol/gel route and oxalic with platelet morphology. A second kinetics, slower with about 1.6 %.min^{-1} corresponds to the sample calcined under reductive atmosphere. The third kinetics starts with an induction period of 30 min with almost no dissolution, followed by similar dissolution kinetics than the two first samples. It is this last value retained to quantify the dissolution kinetics for this sample.

This project has received funding from the EURATOM research and training programme 2014-2018 under grant agreement No 755171. The content of this deliverable reflects only the author's view. The European Commission is not responsible for any use that may be made of the information it contains.

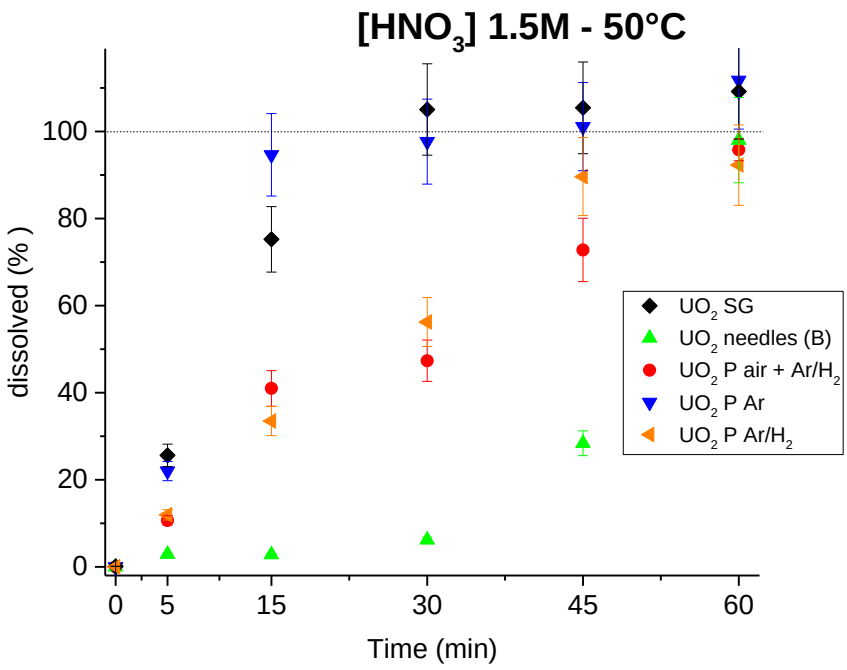

Figure 17 : Dissolution of five UO_2 powders, in 1.5 mol.L^{-1} nitric acid at 50°C

Once again, same partial orders for the crystallite size and the specific surface area than determined in PuO_2 and $U_{0.39}Pu_{0.61}O_2$ models (ie -1 and 0.33 respectively) were kept constant, the resolution of the system of five equations with an unknown leads to the empirical law Equation 5. The correlation coefficient of this law is only of 0.70. However, deviations between modelled and experimental kinetics, reported in Table 8 show a good agreement except for the sample calcined in reductive atmosphere. Without this test, the correlation coefficient increases to 0.91 more satisfying. Concerning this discarded test, to match with the model crystallite size of 360 nm and SSA of one order of magnitude higher should be necessary, that is just not compatible with SEM observation or with uncertainties of BET method. Probably, experimental dissolution kinetics determination would be unaccurate.

$$r = 10^{2,78} * Tc^{-1} * S_{spé}{}^{0,33} \qquad \text{Equation 5}$$

Table 8 : Experimental and modelled dissolution kinetics of UO_2

UO_2 sample	Experimental dissolution kinetics (%dissolved.min^{-1})	Modelled dissolution kinetics (%dissolved.min^{-1})
Sol-gel	5.0 ± 0.7	4.6 ± 1.1
Platelets Ar	6.1 ± 0.9	5.9 ± 1.4
Needles (B)	5.5 ± 1.1	3.7 ± 0.9
Platelets Ar/H_2	1.6 ± 0.2	3.6 ± 0.8
Platelets Air+Ar/H_2	1.6 ± 0.2	1.7 ± 0.4

This project has received funding from the EURATOM research and training programme 2014-2018 under grant agreement No 755171. The content of this deliverable reflects only the author's view. The European Commission is not responsible for any use that may be made of the information it contains.

DISSOLUTION OF $U_{0,75}PU_{0,25}O_2$ SAMPLES:

The different $U_{0,75}Pu_{0,25}O_2$ powders were dissolved in similar conditions than UO_2. Each sample have a different dissolution kinetics as Figure 18, all three slower than UO_2 dissolution kinetics.

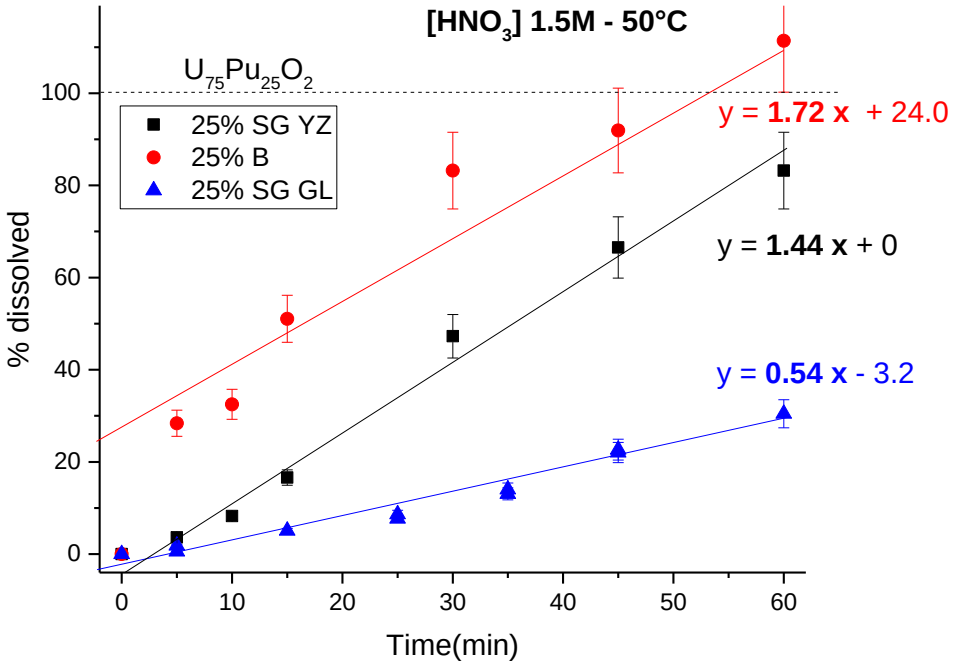

Figure 18 : Dissolution of $U_{0,75}Pu_{0,25}O_2$ powders, in 1.5 mol.L^{-1} nitric acid at 50°C.

Keeping constant the partial orders for crystallite size and SSA, one more time, the resolution of the system of three equations with an unknown leads to the empirical law Equation 6:

$$r = 10^{2,01} * Tc^{-1} * S_{spé}{}^{0,33} \qquad \text{Equation 6}$$

The correlation coefficient of this law is only of 0.93, satisfying, deviations could be due to high uncertainties in crystallite size determinations linked to less quality of XRD plate preparation.

So, whatever the Pu content, it was possible to model the morphological effects on dissolution kinetics using a law such $r = k * SSA^{0,33} * Sc^{-1}$ with k dependent on nitric concentration, temperature, and Pu content.

This project has received funding from the EURATOM research and training programme 2014-2018 under grant agreement No 755171. The content of this deliverable reflects only the author's view. The European Commission is not responsible for any use that may be made of the information it contains.

EFFECT OF PU CONTENT ON DISSOLUTION KINETICS

This extrapolation is applied to all mixed oxides and makes it possible to dissociate, under same experimental conditions, the effects of the plutonium content and the morphological effects.
The experimental conditions of dissolution of all samples of this study were kept constant (i.e. [HNO_3] = 8.5M at 95°C, stirring rate of 300 rpm), in order to look at the specific effect of the plutonium content on dissolution of $(U_{1-x}Pu_x)O_{2\pm\delta}$. The determination of the concentration of plutonium in solution allows reaching the mass of dissolved oxide and thus the percentage of powder dissolved at each instant. All these percentages lead to a linear evolution and the dissolution kinetics rate is obtained by a linear regression of the experimental data. The dissolutions of the different Pu compounds are illustrated in Figure 19. As it has already been reported in the scientific literature, increasing the plutonium content leads to a decrease in kinetics. A factor close to one thousand is observed between the dissolution kinetics of $U_{0.64}Pu_{0.36}O_{2\pm\delta}$ and PuO_2. However here, the dissolution rate of the PuO_2 appears faster than the dissolution rate of the $U_{0.24}Pu_{0.76}O_{2\pm\delta}$, this can be explained by morphological parameters making the PuO_2 powder more favorable to dissolution than the $U_{0.24}Pu_{0.76}O_{2\pm\delta}$ (lower crystallite size and higher specific surface area). The dissolution kinetics rate of the $U_{0.64}Pu_{0.36}O_{2\pm\delta}$ powder is obtained only from two experimental points, because of a high reactivity of this powder. Table 2 and Table 3 present similar morphological parameters for the studied compounds, with only a factor of 4 between the smallest and largest crystallites size and a factor of 15 between the lowest and highest specific surface area. So, there is a consequent effect of the plutonium content on the dissolution kinetics. Some tests were carried out under similar experimental conditions on powders with lower plutonium content (25% and less) but dissolution rates were too fast to be experimentally measured.

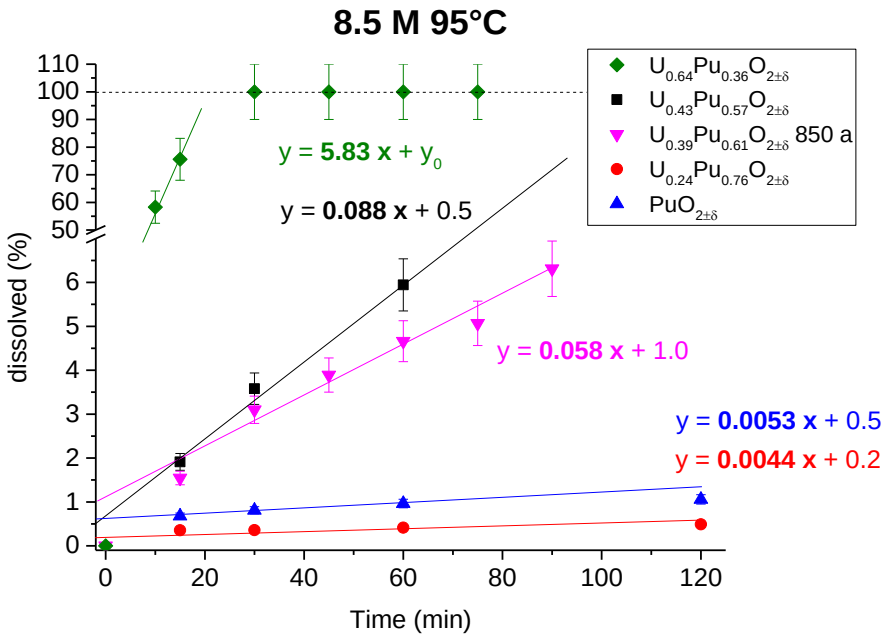

Figure 19 : Dissolution of $(U_{1-x}Pu_x)O_{2\pm\delta}$ powders with different plutonium contents and different morphologies in the same experimental conditions ([HNO_3]=8.5mol.L^{-1} at 95°C).

Under same experimental conditions and after having understood the effect that the morphology induces on dissolution kinetics, it is then possible to quantify the effect of the plutonium content of the oxide on its dissolution kinetics rate in nitric acid 8.5M at 95°C determining each k value for the different plutonium contents studied. The different k values are summarized in Table 9, column “experiment k”. By plotting the

This project has received funding from the EURATOM research and training programme 2014-2018 under grant agreement No 755171. The content of this deliverable reflects only the author’s view. The European Commission is not responsible for any use that may be made of the information it contains.

logarithmic functions of the constant k according to the plutonium content, a line is obtained (Figure 20) defining by the regression presented in Equation 7, k value for the Pu content of 57 % was not taken into account for this linear regression in order to be used as a validation point. This empiric law defines an effect of Pu content on dissolution kinetics following an exponential function for a range of Pu content between 36 and 100 % similar to the findings of Ikeuchi [3] on the range of 18 to 29 %.

Table 9 : k values depending on Pu content of $(U_{1-x}Pu_x)O_{2\pm\delta}$ for dissolution in nitric acid 8.5M at 95°C

%Pu	Log %Pu	experiment k	Log k
36	1.56	374.00	2.57
61	1.79	0.19	-0.72
		2.53	0.40
		2.60	0.41
76	1.88	1.58	0.20
100	2.00	0.05	-1.30
57	1.76	7.04	0.85

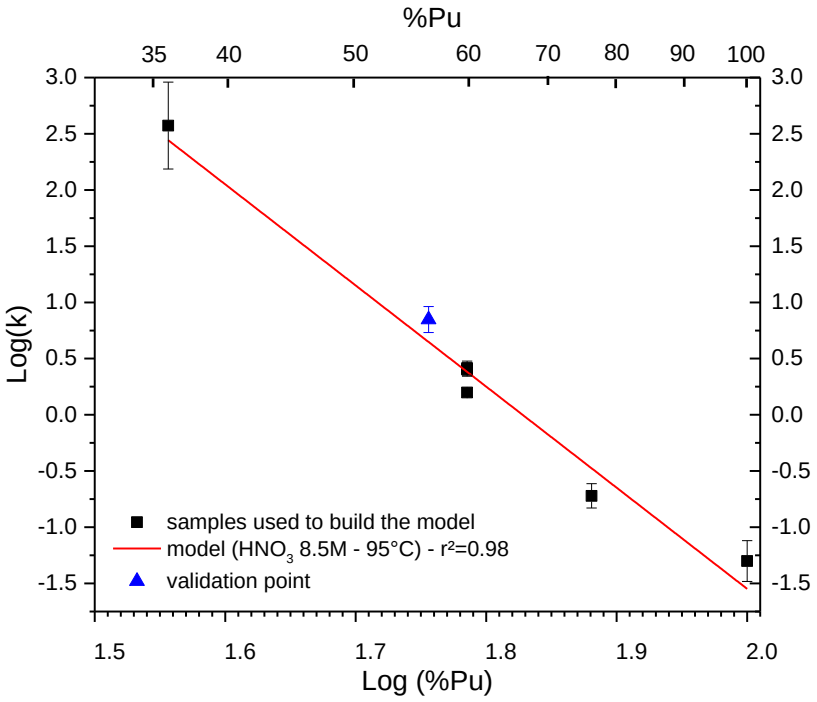

Figure 20: Relation between the kinetic rate constant and the plutonium content of the oxide at 8.5 mol.L^{-1} heated at 95°C.

$$k = \%Pu^{-9.0} * 10^{-16.4}$$ **Equation 7**

With %Pu the plutonium content of the oxide powder in percent.

It has to be noticed than between the two limits of the tested interval (36 % and 100 % of Pu) the dissolution kinetics rate is multiplied by almost 7500. Looking at the validation point, the model k value for 57 % of Pu is 4.44 for an experiment value of 7.04, so a difference of only 37 %. Therefore, it is possible to conclude that the effect of the plutonium content on the dissolution kinetics could be defined by a power function. As

This project has received funding from the EURATOM research and training programme 2014-2018 under grant agreement No 755171. The content of this deliverable reflects only the author's view. The European Commission is not responsible for any use that may be made of the information it contains.

mentioned, the parameters of the function are only valid for dissolution in nitric acid 8.5M at 95°C. The next step of such study should be to look at the effect of acidity and temperature on the different parameters of the laws used, in order to be able to define a general law modelling the dissolution of $(U_{1-x}Pu_x)O_{2\pm\delta}$ whatever the morphologic properties of the powder, its composition (plutonium content) and the dissolution conditions (acidity and temperature).

CONCLUSION

Eighteen different actinide samples were synthetized in order to be able to study dissolution in function of morphology and Pu amount. The characterization tools employed in this study were used to describe the plutonium content and the morphology of the different powders. It appears that the specific surface area decreases and the crystallite size increases while the calcination temperature increases too, in agreement with literature data.

For several Pu contents, several samples were prepared, presenting different morphologies. Each time, a kinetic law has been validated allowing to describe with precision the effect induced by the morphology on the dissolution rates. Although the physical relationship existing between the dissolution rates and the described morphological properties has not yet been described, mathematically there seems to be a close link between specific surface area, crystallite sizes and the dissolution kinetics of the oxide powders whatever the Pu contents or the dissolution media, these two being included in the constant of the morphologic law.

Finally, dissolution kinetics using the same experimental conditions indicate a decrease in dissolution kinetics while the plutonium content increases too. Despite a difference of a factor of about 7500 between the dissolution kinetics of $U_{0,64}Pu_{0,36}O_{2\pm\delta}$ and PuO_2, an empirical law could be established and validated describing the effect of the plutonium content on dissolution rates at 8.5 $mol.L^{-1}$ 95°C.

This project has received funding from the EURATOM research and training programme 2014-2018 under grant agreement No 755171. The content of this deliverable reflects only the author's view. The European Commission is not responsible for any use that may be made of the information it contains.

REFERENCES

[1] A.L.Uriarte, R.H.Rainey, Dissolution of high-density UO2, PuO2, and UO2-PuO2 pellets in inorganic acids, ORNL-3695, 1965.

[2] R.E.Lerch, Dissolution of unirradiated mechanically blended, sol gel, and coprecipitated mixed oxide fuel, HEDL-TME 72-67, 1972.

[3] H. IKeuchi, A. Shibata, Y. Sano, T. Koizumi, Dissolution of irradiated mixed-oxide fuels with different plutonium contents, Procedia Chemistry 7 , 77-83, 2012.

[4] D.Vollath, H.Wedemeyer, On the dissolution of (U,Pu)O2 solid solutions with different Pu contents in boiling nitric acid, Nuclear technology 71, 1985.

[5] G.F.Molen, Dissolution of Plutonium Oxide, RFP-922, UC-4 Chemistry, TID-4500, 1967.

[6] Vaidya V.N Sol-gel process for ceramic nuclear fuels. Journal of Sol-Gel Science and Technology, 369-381, 2008.

[7] K-C Jeong, Y-K Kim, S-C Oh, M-S Cho, Y-W Lee, and J-W Chang, UO3 Intermediate Particle Preparation Using the Sol-Gel Process, Transactions of the Korean Nuclear Society Autumn Meeting Busan, Korea, October 27-28,2005.

[8] http://www.chemguide.co.uk/physical/phaseeqia/nonideal.html. Site consulté le 25 avril 2017.

[9] DIFFRACplus TOPAS/TOPAS R/TOPAS P Version 2.1 and www.bruker-axs.com.

[10] Cheary R.W, Coelho A.A, Cline J.P (2004) Fundamental parameters line profile fitting in laboratory diffractometers. J. Res. Natl. Inst. Stand. Technol. 109, 1-25.

[11] W.J. Young, L. Lynds. An X-Ray and density study of nonstoichiometry in uranium oxides. Atomic International (USA) report, NAA-SR-6765, 1962.

[12] A.J. Freeman, J.B. Darby Jr, The actinides – Electronic structure and related properties, Vol II, Material Science Series, ISBN 0-12-266702-6, 1974.

[13] B. Arab-Chapelet, F. De Bruycker, S. Picart, G. Leturcq, S. Grandjean, Structural characterization of mixed uranium-plutonium co-precipitates and oxides synthesized by oxalic co-conversion route, ATALANTE 2008, Montpellier, 19-22 May 2008.

[14] X.Machuron-Mandard, Etude de la cinétique et du mécanisme de la réaction de dissolution du bioxyde de plutonium par l'ion Cr (II) en solution acide, Thèse de doctorat, Université Paris VI, 1991.

[15] Y.B. Rao, R.B. Yadav, R.N. Swamy, B. Gopalan, S. Syamsundar, Determination of specific surface area of uranium oxide powders using differential thermal analysis technique, Journal of thermal analysis vol 44, pages 1439-1448, 1995.

[16] C. Ganguly, R.N. Jayaraj, Characterisation and quality control of nuclear fuels. ISBN 81-7764-608-7, 2004

This project has received funding from the EURATOM research and training programme 2014-2018 under grant agreement No 755171. The content of this deliverable reflects only the author's view. The European Commission is not responsible for any use that may be made of the information it contains.